


T_{cc}^+ and $\chi_{c1}(3872)$ with the complex scaling method and $DD(\bar{D})\pi$ three-body effect

Zi-Yang Lin^{⊗,*}, Jian-Bo Cheng^{⊗,†} and Shi-Lin Zhu^{⊗,‡}

School of Physics and Center of High Energy Physics, Peking University 10087, China

 (Received 7 March 2024; accepted 13 August 2024; published 9 September 2024)

We use the leading-order contact interactions and one-pion-exchange potentials to investigate the newly observed double-charm state T_{cc}^+ . We employ the complex scaling method to search for the poles on the first Riemann sheet with respect to the DD^* threshold and the second Riemann sheet with respect to the $DD\pi$ threshold. The $DD\pi$ three-body effect is important in this system since the intermediate states can go on shell. We involve the three-body effect through an energy-dependent one-pion-exchange potential, which results in a unitary cut at the $DD\pi$ three-body threshold. We find a pole corresponding to the T_{cc}^+ on the physical Riemann sheet. Its width is around 80 keV and nearly independent of the choice of the cutoff. Assuming the $D\bar{D}\pi$ and $D\bar{D}^*$ channels as the main decay channels, we apply the similar calculations to the $\chi_{c1}(3872)$, and find its width is even smaller. The isospin breaking effect is so significant for the $\chi_{c1}(3872)$ that it is mainly a molecular state of $D^0\bar{D}^{*0}$. Furthermore, we introduce a revised Schrödinger equation for unstable particles to include the contribution of the D^* width, which is also revised by the three-body effect.

DOI: [10.1103/PhysRevD.110.054008](https://doi.org/10.1103/PhysRevD.110.054008)

I. INTRODUCTION

Recently, the LHCb collaboration observed a double-charm exotic hadron with $J^P = 1^+$ named as T_{cc}^+ in the $D^0D^0\pi^+$ mass spectrum, and its mass and width are [1]

$$\delta m_{\text{BW}} = -273 \pm 61 \text{ keV}, \quad \Gamma_{\text{BW}} = 410 \pm 165 \text{ keV}, \quad (1)$$

where δm_{BW} is the T_{cc}^+ mass shift with respect to the D^0D^{*+} threshold and Γ denotes its width. This result is extracted from a relativistic P-wave two-body Breit-Wigner parametrization and is only a rough description of the state. Since the state is rather close to the D^0D^{*+} threshold, a further study is carried out using a unitarized Breit-Wigner parametrization, which gives [2]

$$\delta m_{\text{U}} = -359 \pm 40 \text{ keV}, \quad \Gamma_{\text{U}} = 47.8 \pm 1.9 \text{ keV}. \quad (2)$$

The pole position is also derived from the same unitarized Breit-Wigner parametrization,

$$\delta m_{\text{pole}} = -360 \pm 40 \text{ keV}, \quad \Gamma_{\text{pole}} = 48 \pm 2 \text{ keV}. \quad (3)$$

*Contact author: lzy_15@pku.edu.cn

†Contact author: jbcheng@pku.edu.cn

‡Contact author: zhusl@pku.edu.cn

Published by the American Physical Society under the terms of the Creative Commons Attribution 4.0 International license. Further distribution of this work must maintain attribution to the author(s) and the published article's title, journal citation, and DOI. Funded by SCOAP³.

The pole position is directly related to theoretical calculations based on dynamical models and the Schrödinger equation.

Another important feature of the T_{cc}^+ is the absence of signals in the D^+D^{*+} and $D^+D^0\pi^+$ mass spectra. It implies that the T_{cc}^+ is an isoscalar rather than an isovector, which is similar to the charmoniumlike exotic state $\chi_{c1}(3872)$ [$X(3872)$] first observed in 2003 [3], with the spin-parity quantum number $J^{PC} = 1^{++}$ and isospin $I = 0$. Since the $\chi_{c1}(3872)$ lies so close to the $D^0\bar{D}^{*0}$ threshold, the LHCb collaboration made a more precise investigation of its line shape in 2020 [4]. The generic Breit-Wigner mass and width are

$$m_{\chi_{c1}(3872)} = 3871.695 \pm 0.067 \pm 0.068 \pm 0.010 \text{ MeV}, \\ \Gamma_{\text{BW}} = 1.39 \pm 0.24 \pm 0.10 \text{ MeV}. \quad (4)$$

A fit with the Flatté line shape, which better describes near-threshold resonances, is also carried out, and the peak position and the full width of the half maximum is

$$\text{mode} = 3871.69_{-0.04-0.13}^{+0.00+0.05} \text{ MeV}, \\ \text{FWHM} = 0.22_{-0.06-0.13}^{+0.07+0.11} \text{ MeV}. \quad (5)$$

The pole search is also done, and a pole on the first (physical) Riemann sheet with respect to the $D^0\bar{D}^{*0}$ threshold is preferred. At the best estimate of the Flatté parameters, the pole position is found to be

$$E = 0.06 - 0.13i \text{ keV}, \quad (6)$$

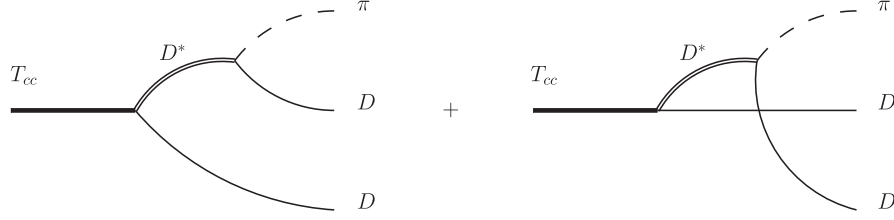


FIG. 1. T_{cc}^+ decaying to $DD\pi$. There are two diagrams due to the identical particles. The interference contributes to the three-body effect in the OPE.

where the imaginary part of the pole position corresponds to the opposite of half the width. Notice that the generic Breit-Wigner parametrization does not work for near-threshold states. (See the review “Resonances” in Ref. [5].) Hereinafter we always focus on the pole positions.

A variety of works studied the double-charm and hidden-charm tetraquarks. There are several theoretical interpretations for the double-charm tetraquarks: the molecular state picture [6–17], the compact tetraquark picture [18–25], the QCD sum rule [26], and the lattice QCD simulation [27,28]. As for the hidden-charm $\chi_{c1}(3872)$, see Refs. [29–34] for a detailed review.

In this work, we regard the $T_{cc}^+[\chi_{c1}(3872)]$ as a loosely bound $DD^*(D\bar{D}^*)$ molecular state. The chiral effective field theory (ChEFT) serves as a helpful tool to study this system since the momenta of the charmed mesons are small. Based on Weinberg’s power counting [35,36], the calculations can be organized by the powers of the small external momenta and pion mass. In the ChEFT, the one-pion-exchange (OPE) potential provides the long-range attraction. Together with the intermediate-range interactions from the two-pion-exchange (TPE) and short-range interactions from the contact terms, the ChEFT provides a successful description of the nucleon systems [37–39]. Similar to the heavy baryon chiral effective field theory used in the nucleon systems [40], the heavy meson chiral effective field theory (HMChEFT) is performed to deal with the charmed mesons [41]. For a review of the ChEFT for heavy hadronic molecules, see Ref. [42].

However, the DD^* system is somehow extraordinary because the mass splitting between the pseudoscalar meson D and the vector meson D^* is slightly larger than the pion mass in most cases except for the D^{*0} and D^+ . Therefore, the exchanged pion can go on shell, which calls for a calculation satisfying the three-body unitarity. According to the optical theorem, the on-shell $DD\pi$ intermediate state introduces an imaginary part to the potential, leading to a nonvanishing width of DD^* bound states above the $DD\pi$ threshold. As we will see, the Hamiltonian is no longer Hermitian, which results in the complex energy eigenvalues.

Given $DD\pi$ is the only kinematically permitted strong decay mode of T_{cc}^+ , the three-body unitarity is very important in describing the property of T_{cc}^+ , especially its extremely narrow width. In a nonperturbative calculation, three-body states should be included in the two-body

iterative equations. As depicted in Fig. 1, there are two Feynman diagrams for the T_{cc}^+ decay at tree level due to the final-state identical bosons.¹ The interference of the two diagrams gives rise to the OPE in the DD^* scattering, while the square of modulus of a single diagram gives rise to the D^* self-energy. One can expect that these two three-body effects, arising from the OPE and the D^* width, respectively, are comparable. Notably, the imaginary part of the potential is proportional to the three-body decay width, which scales as two-body phase space rather than three-body phase space because the diagrams in Fig. 1 are cascade decays without final-state interactions. The D^* propagator in the three-body decay amplitude constrains the momenta of the final state $D\pi$.

In the literature, the three-body effects have been discussed via the time-ordered perturbation theory in the framework of quantum mechanics [43–45]. A nonrelativistic propagator $(E - H_0 + i\epsilon)^{-1}$ introduces the three-body unitary cut, where the E denotes the center-of-mass energy, and the H_0 denotes the total kinetic energy of the intermediate $DD\pi$ states. Thus the OPE potentials become energy dependent. It was found that the static pion approximation with a constant D^* width, overestimates the width of T_{cc}^+ . As we will see, the energy dependence of the potential is directly related to the three-body component of T_{cc}^+ .

Though a nonrelativistic treatment for pions may be appropriate for loosely bound states, whose relative momenta are small, we shall keep the relativistic form of pions in the spirit of the ChEFT. Thus we keep the relativistic pion propagators but introduce the energy dependence in the zeroth component of the exchanged pion momentum. Then the three-body threshold effect and the width of T_{cc}^+ appear naturally. In this work, we treat the D and D^* mesons nonrelativistically, while the heavy meson recoil corrections are investigated. One can anticipate that the recoil effects are suppressed by $1/M_{D^{(*)}}$ and the pion dynamics matters.

¹If the final-state particles are fermions, then there will be an extra (-1) between the two diagrams. This implies the imaginary part of the OPE may be positive, which reduces the width induced by the self-energy. This does not contradict the optical theorem since the final-state fermions with the same momenta (which is required in the forward scattering amplitude) are forbidden.

The on-shell pion manifests as a pole in the OPE potential, or a logarithmic singularity in the partial-wave OPE potential. In this case, T_{cc}^+ is actually a $DD\pi$ resonance, and the conventional Schrödinger equation fails to derive such a resonance. To avoid this singularity, we use the complex scaling method (CSM). The CSM is a similarity transformation of the Schrödinger equation [46,47], which allows us to obtain the bound states and resonances in the complex plane simultaneously. For a review of applications of the CSM in the nucleus systems, see Ref. [48]. As a tool of analytical continuation, the CSM can help deal with the singularity of the potential and study the property of resonance wave functions.

This paper is organized as follows. In Sec. II, we introduce the chiral Lagrangians, the complex scaling method and the classification of the poles related to the CSM. We explain why we revise the OPE potential and how to handle the analytical continuation correctly. In Sec. III, we present the effective potentials explicitly, with the isospin breaking effect. In Sec. IV A, we start from the simple isospin conservation case to show how our scheme interacts with the three-body threshold. In Secs. IV B and IV C, we include the isospin breaking effect and present the results of the T_{cc}^+ and $\chi_{c1}(3872)$. In Sec. IV D, we study the corrections from the heavy meson kinetic energies and summarize the numerical results. In Sec. IV E, we investigate the influence of the D^* width on the widths of the T_{cc}^+ and $\chi_{c1}(3872)$. In Sec. V, we make a summary.

II. FORMALISM

A. Chiral Lagrangian

In the HMChEFT, the Lagrangians, together with the scattering amplitudes, can be organized in the powers of small external momenta q over a large energy scale $\Lambda_\chi \sim 1$ GeV. The Λ_χ represents the chiral breaking scale. Up to the $\mathcal{O}(p^2)$ amplitudes, we need only the leading-order (LO) Lagrangian for the $H\phi$ interaction

$$\begin{aligned} \mathcal{L}_{H\phi}^{(1)} = & -\langle (iv \cdot \partial H) \bar{H} \rangle + \langle H v \cdot \Gamma \bar{H} \rangle \\ & + g \langle H \not{\psi} \gamma_5 \bar{H} \rangle - \frac{1}{8} \delta \langle H \sigma^{\mu\nu} \bar{H} \sigma_{\mu\nu} \rangle, \end{aligned} \quad (7)$$

where ϕ denotes the Goldstone bosons, and H denotes the heavy meson doublet under the heavy quark spin symmetry [41], which is defined as

$$\begin{aligned} H &= \frac{1 + \not{v}}{2} (P_\mu^* \gamma^\mu + iP \gamma_5), \\ \bar{H} &= \gamma^0 H^\dagger \gamma^0 = (P_\mu^{*\dagger} \gamma^\mu + iP^\dagger \gamma_5) \frac{1 + \not{v}}{2}, \\ P &= (D^0, D^+), \quad P_\mu^* = (D^{*0}, D^{*+}). \end{aligned} \quad (8)$$

The last term in Eq. (7) introduces the mass splitting between heavy pseudoscalar and vector mesons, and

$v = (1, \vec{0})$ is the four velocity of the heavy mesons. The chiral connection Γ_μ and the axial current u_μ contain an even and odd number of the Goldstone bosons, respectively, which read

$$\begin{aligned} \Gamma_\mu &= \frac{i}{2} [\xi^\dagger, \partial_\mu \xi] = -\frac{1}{4f_\pi^2} \epsilon^{abc} \tau^c (\phi^a \partial_\mu \phi^b) + \dots, \\ u_\mu &= \frac{i}{2} \{ \xi^\dagger, \partial_\mu \xi \} = -\frac{1}{2f_\pi} \tau^a \partial_\mu \phi^a + \dots, \\ \xi &= \exp(i\phi/2f_\pi), \\ \phi &= \phi^a \tau^a = \sqrt{2} \begin{pmatrix} \frac{\pi^0}{\sqrt{2}} & \pi^+ \\ \pi^- & -\frac{\pi^0}{\sqrt{2}} \end{pmatrix}, \end{aligned} \quad (9)$$

where λ^a denotes the Pauli matrices, and f_π represents the decay constant of the Goldstone bosons.

The next-to LO $H\phi$ Lagrangian $\mathcal{L}_{H\phi}^{(2)}$ contains at least two light mesons, which only appears in the TPE diagrams and thus does not contribute to the $\mathcal{O}(p^2)$ amplitudes.

To mimic the short-range interactions between the heavy mesons, we need the contact Lagrangian with low-energy constants (LEC)

$$\begin{aligned} \mathcal{L}_{4H}^{(0)} &= D_a \text{Tr}[H \gamma_\mu \bar{H}] \text{Tr}[H \gamma^\mu \bar{H}] \\ &+ D_b \text{Tr}[H \gamma_\mu \gamma_5 \bar{H}] \text{Tr}[H \gamma^\mu \gamma_5 \bar{H}] \\ &+ E_a \text{Tr}[H \gamma_\mu \tau^a \bar{H}] \text{Tr}[H \gamma^\mu \tau^a \bar{H}] \\ &+ E_b \text{Tr}[H \gamma_\mu \gamma_5 \tau^a \bar{H}] \text{Tr}[H \gamma^\mu \gamma_5 \tau^a \bar{H}]. \end{aligned} \quad (10)$$

For the $D\bar{D}^*$ system, the Lagrangian is constructed as follows:

$$\begin{aligned} \mathcal{L}_{4H}^{(0)} &= 2\tilde{D}_a \text{Tr}[\tilde{H} \gamma_\mu \tilde{H}] \text{Tr}[H \gamma^\mu \bar{H}] \\ &+ 2\tilde{D}_b \text{Tr}[\tilde{H} \gamma_\mu \gamma_5 \tilde{H}] \text{Tr}[H \gamma^\mu \gamma_5 \bar{H}] \\ &+ 2\tilde{E}_a \text{Tr}[\tilde{H} \gamma_\mu \tau^a \tilde{H}] \text{Tr}[H \gamma^\mu \tau^a \bar{H}] \\ &+ 2\tilde{E}_b \text{Tr}[\tilde{H} \gamma_\mu \gamma_5 \tau^a \tilde{H}] \text{Tr}[H \gamma^\mu \gamma_5 \tau^a \bar{H}], \end{aligned} \quad (11)$$

$$\begin{aligned} \mathcal{L}_{\tilde{H}\phi}^{(1)} &= -\langle (iv \cdot \partial \tilde{H}) \tilde{H} \rangle + \langle \tilde{H} v \cdot \Gamma \tilde{H} \rangle \\ &+ g \langle \tilde{H} \not{\psi} \gamma_5 \tilde{H} \rangle - \frac{1}{8} \delta \langle \tilde{H} \sigma^{\mu\nu} \tilde{H} \sigma_{\mu\nu} \rangle, \end{aligned} \quad (12)$$

where \tilde{H} stands for the heavy antimeson fields

$$\begin{aligned} \tilde{H} &= (\tilde{P}_\mu^* \gamma^\mu + i\tilde{P} \gamma_5) \frac{1 - \not{v}}{2}, \\ \tilde{\bar{H}} &= \gamma^0 H^\dagger \gamma^0 = \frac{1 - \not{v}}{2} (\tilde{P}_\mu^{*\dagger} \gamma^\mu + i\tilde{P}^\dagger \gamma_5), \\ \tilde{P} &= \begin{pmatrix} \tilde{D}^0 \\ \tilde{D}^- \end{pmatrix}, \quad \tilde{P}_\mu^* = \begin{pmatrix} \tilde{D}^{*0} \\ \tilde{D}^{*-} \end{pmatrix}. \end{aligned} \quad (13)$$

Note that the heavy meson scheme spoils the crossing symmetry, so the LECs in Eqs. (10) and (11) are not exactly the same. In Eqs. (10)–(11), we have merged terms like $\text{Tr}[H\bar{H}]\text{Tr}[H\bar{H}]$ and $\text{Tr}[H\gamma_\mu\bar{H}]\text{Tr}[H\gamma^\mu\bar{H}]$, since they are not independent after the heavy meson reduction. However, they do get an extra opposite sign under the charge conjugation, which accounts for the differences between the LECs for DD^* and $D\bar{D}^*$ systems.

Besides, we could introduce an imaginary part to the LECs in Eq. (11) to involve the annihilation effects and contributions from the inelastic channels.

In principle, the higher order contact terms $L_{4H}^{(2)}$ should be included to cancel the divergences of the loop integrals. Although these terms do contribute to the $\mathcal{O}(p^2)$ amplitudes, we ignore their finite part due to the lack of the experimental data.

Due to proximity to the $DD\pi$ three-body threshold, the heavy meson kinetic energies may have a considerable contribution which reduces phase space. In this work, we first calculate the effective potentials under the heavy meson limit in the framework of HMChEFT. Then we include the $1/M_{D^{(*)}}$ corrections to evaluate the recoil corrections of the heavy meson.

B. Effects of the three-body threshold

As explained in Fig. 1, there are two aspects of three-body effects which influence the width of the T_{cc}^+ or $\chi_{c1}(3872)$: the OPE potential and the D^* width.

It is noteworthy that what we are discussing is in fact a three-body “kinematic” effect since the three-body force is not considered. The intermediate three-body states are treated to be free, and they can only interact through their coupling to two-body states.

In the following, we take the OPE potential for example to involve the three-body effect by retaining the energy dependence. A typical OPE potential has the form of

$$\begin{aligned} V_{1\pi} &= C \frac{(\epsilon \cdot p)(\epsilon' \cdot p)}{p^2 - m_\pi^2 + i0+}, \\ &= C \frac{(\epsilon \cdot p)(\epsilon' \cdot p)}{p_0^2 - \mathbf{p}^2 - m_\pi^2 + i0+}, \end{aligned} \quad (14)$$

where p represents the transferred momentum, C is a constant related to the isospin and coupling constants, and ϵ, ϵ' represent the polarization vectors of the initial and final D^* mesons, respectively.

In early works, the instantaneous approximation, namely taking $p_0 = 0$, is performed. This will lead to a Yukawa interaction similar to the nucleon case. Nonetheless, it is inappropriate in the DD^* system, since $\delta = m_{D^*} - m_D$ is comparable to and even larger than the pion mass. If we keep a static pion energy $p_0 \approx m_{D^*} - m_D$ instead, then the OPE potential becomes

$$V_{1\pi} = -C \frac{(\epsilon \cdot p)(\epsilon' \cdot p)}{\mathbf{p}^2 - m_{\text{eff}}^2 - i0+}, \quad (15)$$

$$\text{Im}V_{1\pi} = -\pi C (\epsilon \cdot p)(\epsilon' \cdot p) \delta(\mathbf{p}^2 - m_{\text{eff}}^2). \quad (16)$$

where the effective mass is defined as $m_{\text{eff}}^2 = \delta^2 - m_\pi^2 > 0$.

A pole singularity shows up in the OPE potential, which brings a nonvanishing imaginary part to the potential and makes the potential non-Hermitian. Some of the previous works [49,50] kept the nonvanishing p^0 above but dropped the imaginary part of the potential through a principal integral when performing the Fourier transformation to the coordinate space. The potential in coordinate space oscillates after the Fourier transformation [51,52]. This approach can only derive the approximate binding energy but cannot derive the width.

Even if one retains the imaginary part of the potential, the behavior near the three-body threshold is still not correct. Compared with the instantaneous approximation, the OPE potential with a nonzero imaginary part will lead to a nonzero width of the bound state. However, the pole would have a nonvanishing imaginary part even below the three-body threshold.

So here we need to keep both the imaginary part and the energy dependence of the OPE potential to involve the $DD\pi$ three-body effect. According to the optical theorem, the imaginary part of the OPE potential is related to the three-body final state $DD\pi$ and the width arises from the decay mode $DD\pi$, as depicted in Fig. 2. So we revise the OPE potential as

$$V_{1\pi} = C \frac{(\epsilon \cdot p)(\epsilon' \cdot p)}{(E + \delta)^2 - \mathbf{p}^2 - m_\pi^2 + i0+}, \quad (17)$$

where δ is the mass splitting between the D^* and D mesons, and E is the energy with respect to the DD^* threshold, which is shifted compared with the notation in Fig. 2.

The imaginary part of Eq. (17) is proportional to the three-body decay width, and consistent with Refs. [43–45] under the nonrelativistic limit. This potential is coincident

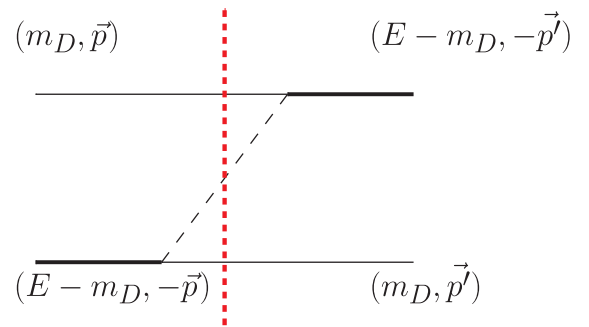


FIG. 2. The one-pion-exchange diagram. The on-shell intermediate state contributes to the imaginary part of the potential. E denotes the center-of-mass energy.

with a reduced coupled-channel calculation. In the coupled-channel cases, the coupling to a lower channel will bring in an extra imaginary part to the effective potential of the higher channel. For a review of the potential with a reduced channel, see Ref. [53].

Since $\delta > m_\pi$, we will encounter logarithmic divergences if performing the integral along the real axis. A unitary cut is introduced to the potential from $E = -\delta + m_\pi$ to $+\infty$. As shown in Fig. 3, the integral over $|p|$ is defined along the positive real axis. When E changes, the pole at $p = \sqrt{(E + \delta)^2 - m_\pi^2}$ may cross the positive real axis and cause discontinuity. The discontinuity exists only when $\text{Re}(\sqrt{(E + \delta)^2 - m_\pi^2}) > 0$. This is the origin why the potential has a branch point at the lower threshold $E = -\delta + m_\pi$. As indicated in Ref. [2], the pole of the T_{cc}^+ state lies on the second Riemann sheet with respect to the $DD\pi$ threshold. To correctly put the potential onto the second Riemann sheet, we use the brown line as the integral path in Fig. 3 instead of the blue one.

Similarly, the other aspect of the three-body effect is introduced via a dynamical D^* width [45,54], which is in principle derived from the D^* self-energy. The imaginary part of the D^* self-energy is finite but its real part diverges. Therefore, its real part depends on the regularization method. For resonances, the real part of D^* self-energy $\Sigma(E)$ may also influence the width of the T_{cc}^+ , since E is a complex number.

Assuming the variation of its real part is small, the dynamical D^* width $\Gamma(E)$ is proportional to the $D\pi$ two-body phase space

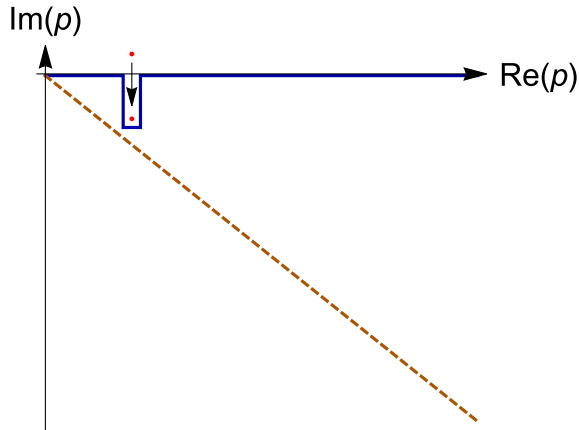


FIG. 3. The integral path from 0 to ∞ in the complex p plane. The red point denotes the pole of the potential located at $p = \sqrt{(E + \delta)^2 - m_\pi^2}$. When the pole passes across the positive real axis, we need to change the integral path to maintain the analytical continuity (blue solid curve). Instead, we can carry out a complex scaled integral (brown dashed curve) to deal with the pole.

$$\begin{aligned} \Gamma_{D^{*+}}(E) &= \frac{g^2 m_{D^0}}{12\pi f_\pi^2 m_{D^{*+}}} k_{D^0\pi^+}^3 + \frac{g^2 m_{D^+}}{24\pi f_\pi^2 m_{D^{*+}}} k_{D^+\pi^0}^3, \\ \Gamma_{D^{*0}}(E) &= \frac{g^2 m_{D^0}}{24\pi f_\pi^2 m_{D^{*0}}} k_{D^0\pi^0}^3, \end{aligned} \quad (18)$$

where E is the total energy of the system. Note that the D^* is off shell and its width is dependent on E .

The final state momenta $k_{D^0\pi^+}$, $k_{D^+\pi^0}$, and $k_{D^0\pi^0}$ can be expressed by the off-shell energy of D^* in its rest frame,

$$\begin{aligned} k_{ij}^2 &= \left(\frac{E_{D^*}^2 - m_i^2 - m_j^2}{2E_{D^*}} \right)^2 - \frac{m_i^2 m_j^2}{E_{D^*}^2} \\ &\xrightarrow{\text{nonrelativistic}} 2 \frac{m_i m_j}{m_i + m_j} (E_{D^*} - m_i - m_j), \end{aligned} \quad (19)$$

where $i = D^+, D^0$, $j = \pi^+, \pi^0$, and E_{D^*} is the energy of D^* in its rest frame, $E_{D^*} = [(E - \sqrt{p^2 + m_D^2})^2 - p^2]^{1/2} \approx E - m_D - \frac{p^2}{2\mu}$ where $\mu = \frac{m_D m_{D^*}}{m_D + m_{D^*}}$. At the leading order, $k_{ij} \propto (E - m_i - m_j)^{3/2}$.

C. Complex scaling method

Once deriving the effective potentials, we can search for the possible bound states or resonances using the CSM. We consider the Schrödinger equation in momentum space

$$E\phi_l(p) = \frac{p^2}{2\mu} \phi_l(p) + \int \frac{p'^2 dp'}{(2\pi)^3} V_{l,l'}(p, p') \phi_{l'}(p'), \quad (20)$$

and perform the complex scaling operation

$$p \rightarrow p e^{-i\theta}, \quad \tilde{\phi}_l(p) = \phi_l(p e^{-i\theta}). \quad (21)$$

Then we derive the complex scaled Schrödinger equation with a scaling angle θ

$$\begin{aligned} E\tilde{\phi}_l(p) &= \frac{p^2 e^{-2i\theta}}{2\mu} \tilde{\phi}_l(p) \\ &+ \int \frac{p'^2 e^{-3i\theta} dp'}{(2\pi)^3} V_{l,l'}(p e^{-i\theta}, p' e^{-i\theta}) \tilde{\phi}_{l'}(p'), \end{aligned} \quad (22)$$

where l, l' are the orbital angular momenta, and p denotes the momentum in the center-of-mass frame.

The eigenenergy remains unchanged after the variable substitution in Eq. (21), but with the rotation operation shown above, the poles of the T matrix on the second Riemann sheet can be revealed by solving the complex scaled Schrödinger equation directly. This can be roughly shown using the asymptotic solution in coordinate space

$$\psi(r) \xrightarrow{r \rightarrow \infty} f_l^+(k) e^{-ikr} + f_l^-(k) e^{ikr}. \quad (23)$$

With the complex scaling operation in coordinate space $r \rightarrow re^{i\theta}$, the asymptotic wave function becomes

$$\tilde{\psi}(r) \xrightarrow{r \rightarrow \infty} f_l^+(k)e^{-ikre^{i\theta}} + f_l^-(k)e^{ikre^{i\theta}}. \quad (24)$$

The first term vanishes at the zeros of the Jost function $f_l^+(k)$ which correspond to the poles of the T matrix. We can solve the eigenstates as long as $\tilde{\psi}(r)$ converges at $r \rightarrow \infty$, i.e., $\text{Im } ke^{i\theta} > 0$ or $\text{Arg } k > -\theta$.

A typical distribution of the poles solved by the CSM is shown in Fig. 4. The continuum states line up while the resonances and bound states lie above and below the continuum states, respectively. In the usual cases when the Hamiltonian is Hermitian, the bound states lie accurately on the negative real axis and resonances lie on the

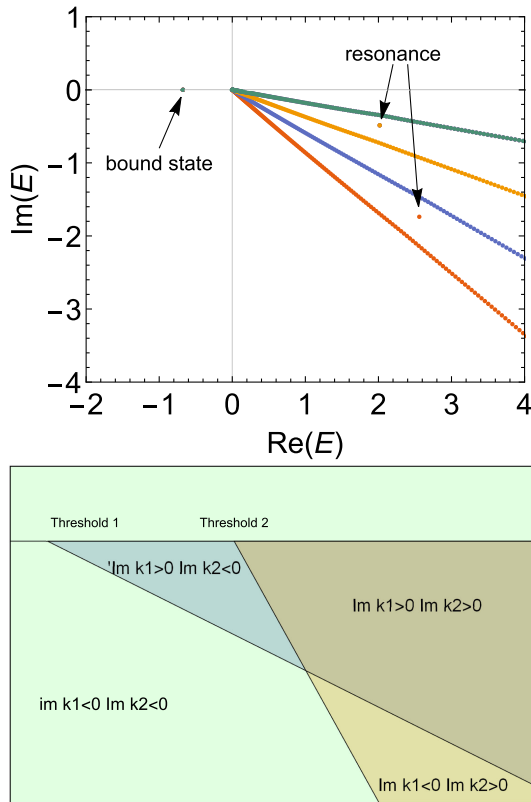


FIG. 4. A typical solution of the complex scaled Schrödinger equation. The green, orange, blue, and red points represent the sets of eigenenergies solved with different complex scaling angles $\theta = 5^\circ, 10^\circ, 15^\circ, 20^\circ$, respectively. The continuum states line up due to the same arguments $\text{Arg}(E) = -2\theta$, while the bound states and resonances are isolated from the line of continuum states and remain static as θ varies. With a Hermitian Hamiltonian, the bound states lie on the negative real axis, while the resonances lie on the fourth quadrant, and can be seen only when $|\text{Arg}(E)| < 2\theta$. The lower figure shows the Riemann sheets in the energy plane in multichannel cases. For different channels, one can choose different rotation angles. The region enclosed by the rotated integral path and the real axis corresponds to the second Riemann sheet rather than the first Riemann sheet.

fourth quadrant. However, the Hamiltonians are no longer Hermitian when we encounter the decay processes. As we will see in Sec. II B, the coupled-channel effects of a lower threshold may introduce a complex potential with a non-vanishing imaginary part, which moves the bound state to the third quadrant. For a precise classification of the poles, see Ref. [53]. These states are called the unstable bound states (or quasibound state in some references). The T_{cc}^+ and $\chi_{c1}(3872)$ locate on the first Riemann sheet with respect to the DD^* threshold, and on the second Riemann sheet with respect to the $DD\pi$ threshold. Thus it can be regarded as a $DD\pi$ resonance and DD^* bound state.

To keep the analytical continuity, one should ensure that the pole in the potential does not cross the integral path during rotation, which demands $\theta > 0$.

The complex scaling method is equivalent to the Lippmann-Schwinger equation. However, it provides a more efficient way to obtain the bound states and resonances simultaneously with no need to calculate the T matrix. Furthermore, we can use CSM to bypass the poles on the real axis when dealing with the OPE potentials.

D. Schrödinger equation for unstable particles

Since D^* decays to $D\pi$, the influence of the D^* width on the width of the DD^* bound state is non-negligible. To include this effect, we first introduce the Schrödinger equation for the bound states of unstable particles, which reads

$$E\phi_l(p) = \left[\frac{p^2}{2\mu} - \frac{i}{2}\Gamma(E) \right] \phi_l(p) + \int \frac{p'^2 dp'}{(2\pi)^3} V_{l,l'}(p, p') \phi_{l'}(p'). \quad (25)$$

The decay width of particles has hardly been included in the Schrödinger equation before. However, the Lippmann-Schwinger equation has been widely used. Equation (25) is established on its equivalence to the following Lippmann-Schwinger equation

$$T(k', k; E) = V(k', k) + \int_0^\infty \frac{p^2 dp}{(2\pi)^3} \frac{V(k', p)T(p, k; k_0)}{E - p^2/2\mu + i\Gamma(E)/2}, \quad (26)$$

in which the Green's function $G(p; E) = \frac{1}{E - p^2/2\mu + i\Gamma(E)/2}$ corresponds to the kinetic energy terms $H_0 = \frac{p^2}{2\mu} - \frac{i}{2}\Gamma(E)$ in Eq. (25). The equivalence of the two equations is briefly explained in Appendix A. In order to involve the three-body effect in the D^* width, $\Gamma(E)$ is treated as a function of the energy rather than a constant.

In Eq. (25), the D meson is treated as a stable particle, and $\Gamma(E)$ denotes the width of D^* , which arises from the self-energy diagram of the D^* . One can make the

replacement $i\Gamma(E) \rightarrow -\Sigma(E)$ to include the influence of the real part of the self-energy. The detailed discussion can be found in Sec. IV E. In multichannel cases, threshold energies must be added to the kinetic term.

III. EFFECTIVE POTENTIAL

Compared with the Born approximation in the scattering, all two-particle-irreducible (2PI) diagrams yield the effective potential

$$V = -\frac{1}{4}\mathcal{M}_{2\text{PI}}, \quad (27)$$

where the factor $-\frac{1}{4}$ differs from the usual $-\prod_i \frac{1}{\sqrt{2M_i}}$ because of the normalization of the heavy meson fields.

Since the ChEFT only works at the small momentum regions, we perform a Gaussian cutoff to regularize the effective potential V , which reads

$$\mathcal{F}(\mathbf{p}, \mathbf{p}') = \exp[-(\mathbf{p}^2 + \mathbf{p}'^2)/\Lambda^2]. \quad (28)$$

We demand $\mathcal{F}(\mathbf{p}, \mathbf{p}') \rightarrow 0$ when $\mathbf{p}, \mathbf{p}' \rightarrow \infty$ before and after the rotation in the complex plane to ensure that the Schrödinger equation can be solved numerically, which constrains the rotation angle $\theta < \pi/4$.

With the isospin symmetry, the potentials in the DD^* system can be obtained through a G-parity transformation. The result is summarized in Table I, where the transferred momentum $p = p_1 - p_4, q = p_1 - p_3$. p_1 and p_3 denote the momenta of the initial and final $D(\bar{D})$ mesons, and p_2 and p_4 stand for the momenta of the initial and final $D^*(\bar{D}^*)$ mesons, respectively. It is interesting to see that the OPE and TPE potentials of T_{cc}^+ and $\chi_{c1}(3872)$ are almost the same.

To simplify the derivation, we only consider the LO potentials, namely the OPE potentials and the LO contact terms. The OPE potential has a generic form

$$V_{1\pi}^i = -\frac{g^2}{4f_\pi^2} \frac{(\boldsymbol{\epsilon} \cdot \mathbf{p})(\boldsymbol{\epsilon}' \cdot \mathbf{p})}{(E + \delta_i)^2 - \mathbf{p}^2 - m_\pi^2 + i0^+}, \quad (29)$$

where E stands for the energy with respect to the lowest two-body threshold and δ_i stands for the mass difference in

TABLE I. The pion-exchange potentials in the DD^* and DD^* system are related by the G-parity transformation. “+” means the potential of the DD^* is the same as that of its partner in the DD^* system with the same isospin, and “-” means an inverse in sign.

	Transfer momentum	G = +	G = -
OPE	p	+	-
TPE	q	+	+
	p	-	+

the i th channel. We have the exchanged pion energy $p^0 = E + m_{\text{th}} - m_{D,i} - m_{D,f}$ from the description in Fig. 2, where m_{th} represents the mass of the threshold. $m_{D,i}$ and $m_{D,j}$ stand for the masses of the initial and final D mesons. For the one-eta-exchange diagrams, the subscript should be changed accordingly.

With the isospin breaking effect included, the coupled-channel potentials are shown as follows. For the DD^* system, we choose $m_{\text{th}} = m_{D^0} + m_{D^{*+}}$, and the OPE potentials are

$$\begin{aligned} V_{D^+D^{*0} \rightarrow D^+D^{*0}} &= -2V_{1\pi^\pm}, \\ \delta_{D^+D^{*0} \rightarrow D^+D^{*0}} &= m_{D^0} + m_{D^{*+}} - 2m_{D^+}, \\ V_{D^+D^{*0} \rightarrow D^0D^{*+}} &= V_{1\pi^0}, \\ \delta_{D^+D^{*0} \rightarrow D^0D^{*+}} &= m_{D^{*+}} - m_{D^+}, \\ V_{D^0D^{*+} \rightarrow D^0D^{*+}} &= -2V_{1\pi^\pm}, \\ \delta_{D^0D^{*+} \rightarrow D^0D^{*+}} &= m_{D^{*+}} - m_{D^0}. \end{aligned} \quad (30)$$

For the DD^* system, we choose the states with the positive C parity

$$\begin{aligned} |[D^+D^{*-}] \rangle &= \frac{1}{\sqrt{2}} (|D^+D^{*-} \rangle - |D^-D^{*+} \rangle), \\ |[D^0\bar{D}^{*0}] \rangle &= \frac{1}{\sqrt{2}} (|D^0\bar{D}^{*0} \rangle - |\bar{D}^0D^{*0} \rangle), \end{aligned} \quad (31)$$

where $[D^+D^{*-}]$ and $[D^0\bar{D}^{*0}]$ are the shorthand notations of the $C = +$ states.

We choose $m_{\text{th}} = m_{D^0} + m_{D^{*0}}$ and then the OPE potentials read

$$\begin{aligned} V_{[D^+D^{*-}] \rightarrow [D^+D^{*-}]} &= -V_{1\pi^0}, \\ \delta_{[D^+D^{*-}] \rightarrow [D^+D^{*-}]} &= m_{D^0} + m_{D^{*0}} - 2m_{D^+}, \\ V_{[D^+D^{*-}] \rightarrow [D^0\bar{D}^{*0}]} &= -2V_{1\pi^\pm}, \\ \delta_{[D^+D^{*-}] \rightarrow [D^0\bar{D}^{*0}]} &= m_{D^{*0}} - m_{D^+}, \\ V_{[D^0\bar{D}^{*0}] \rightarrow [D^0\bar{D}^{*0}]} &= -V_{1\pi^0}, \\ \delta_{[D^0\bar{D}^{*0}] \rightarrow [D^0\bar{D}^{*0}]} &= m_{D^{*0}} - m_{D^0}. \end{aligned} \quad (32)$$

The contribution of the one-eta-exchange potential is quite small and has little influence on the result.

Since we consider only the S-wave interactions, we perform the substitution $(\boldsymbol{\epsilon} \cdot \mathbf{p})(\boldsymbol{\epsilon}' \cdot \mathbf{p}) \rightarrow \frac{1}{3}p^2(\boldsymbol{\epsilon} \cdot \boldsymbol{\epsilon}')$.

The TPE diagrams are provided in the Appendix C.

IV. NUMERICAL RESULTS AND DISCUSSIONS

In this section, we first demonstrate the three-body effect on the pole position in a simple isospin conserved case. Then we successively take into account the isospin breaking effects and the recoil correction to show these effects in

quantity. We leave the D^* width to the last part due to the uncertainty in introducing the D^* self-energy.

We find that the higher order potentials from the TPE diagrams violate the unitarity, and thus are not suitable in this framework. We show the impact of the TPE in Appendix C.

A. Possible bound states with the $\mathcal{O}(p^1)$ DD^* potential

We first use the LO effective potentials only, i.e., the contact and OPE potentials, to show how the CSM works and clarify the T_{cc}^+ pole trajectory near the $DD\pi$ threshold. We choose the average value for the masses: $m_D = 1.867$ GeV, $m_{D^*} = 2.009$ GeV, $m_\pi = 0.139$ GeV. The pion decay constant f_π is chosen as 0.086 GeV and the $DD^*\pi$ coupling constant g is chosen as 0.65 [55]. The isospin conservation is assumed.

In some previous works, the LECs are estimated by the resonance saturation model and quark models, as shown in Table II. For more details on the LECs, see Appendix B. Note that the LECs are dependent on the regulator and the models, which only apply for a limited range of regulators. In this work, we choose the regulator and cutoff in prior and then fix the LECs by fitting the experimental data. Figure 5 shows the pole trajectory as the LEC $C_s = -2D_a + 6E_a$ varies. According to Table II, when we shift C_s from -35 to -19 GeV^{-2} , the pole always lies on the physical Riemann sheet of DD^* , manifesting as a DD^* bound state. When the potential is attractive enough, the pole corresponds to a $DD\pi$ bound state. But when C_s increases, the potential becomes less attractive. The pole moves above the $DD\pi$ threshold and into the unphysical Riemann sheet of the $DD\pi$ threshold. It becomes a $DD\pi$ resonance with a nonvanishing imaginary part. The imaginary part of the pole corresponds to the width decaying to the $DD\pi$ final state. We stress that it is still an unstable bound state of the DD^* whose width arises from its coupling to a lower open

TABLE II. Estimations of LECs with meson-exchange models and quark models (GeV^{-2}). The derivation of LECs are shown in Appendix B.

	Model I ^a	Model II ^b
D_a	-4.4	-2.0
D_b	0	0
E_a	-5.7	-5.9
E_b	0	0
\tilde{D}_a	-6.7	-4.0
\tilde{D}_b	0	0
\tilde{E}_a	-5.7	-12.1
\tilde{E}_b	0	0

^aResonance saturation model [55,56].

^bShort-range quark-quark interactions via the fictitious scalar field and axial-vector field [10,57].

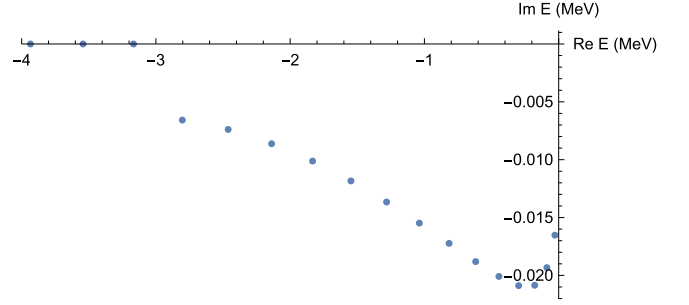


FIG. 5. The pole positions of the bound state in the $I = 0$ S -wave DD^* system with the OPE and contact terms only. When we shift C_s from -35 to -19 GeV^{-2} , the pole moves in the positive real axis direction. With the parameters chosen, the $DD\pi$ threshold is located at -3 MeV. The cutoff Λ is fixed to be 0.5 GeV.

channel. When fixing the real part of the pole to be -0.36 MeV, we have $C_s = -22.3$ GeV^{-2} and the half width is determined to be $\Gamma/2 = 0.021$ MeV.

In general, the LECs depend on the cutoff Λ in Eq. (28) due to the renormalization. But the physical observables are independent of the cutoff chosen. If we change the cutoff and revise C_s accordingly, then it is interesting to see that the width is nearly unchanged, as shown in Table III. The width of the bound state is of the same order of magnitude as the width of the D^* meson. As expected, it is smaller than the D^* width due to the smaller phase space. In addition, no other resonances are found under this set of parameters.

B. Isospin breaking effects

The isospin breaking effect needs to be included carefully because the characteristic energy scale $\delta - m_\pi$ is only several MeV, comparable to the isospin splitting. For example, the mass difference between the D^+ and D^{*0} is 135.8 MeV. They can not exchange the on shell π^+ under the heavy quark limit. Thus the potential in this channel has no singularity.

We perform the coupled-channel calculation involving the D^+D^{*0} and D^0D^{*+} with the parameters listed as follows [5]:

$$\begin{aligned}
 m_{\pi^\pm} &= 0.13957 \text{ GeV}, & m_{\pi^0} &= 0.13498 \text{ GeV}, \\
 m_{D^\pm} &= 1.86966 \text{ GeV}, & m_{D^0} &= 1.86484 \text{ GeV}, \\
 m_{D^{*\pm}} &= 2.01026 \text{ GeV}, & m_{D^{*0}} &= 2.00685 \text{ GeV}.
 \end{aligned} \quad (33)$$

TABLE III. The dependence of the $I = 0$ DD^* contact interaction C_s on the cutoff Λ when the binding energy is fixed to the experimental value. Then the width is calculated using the determined C_s .

Λ (GeV)	C_s (GeV^{-2})	$\Gamma/2$ (MeV)
0.5	-22.3	0.021
0.6	-15.7	0.019
0.7	-11.1	0.019

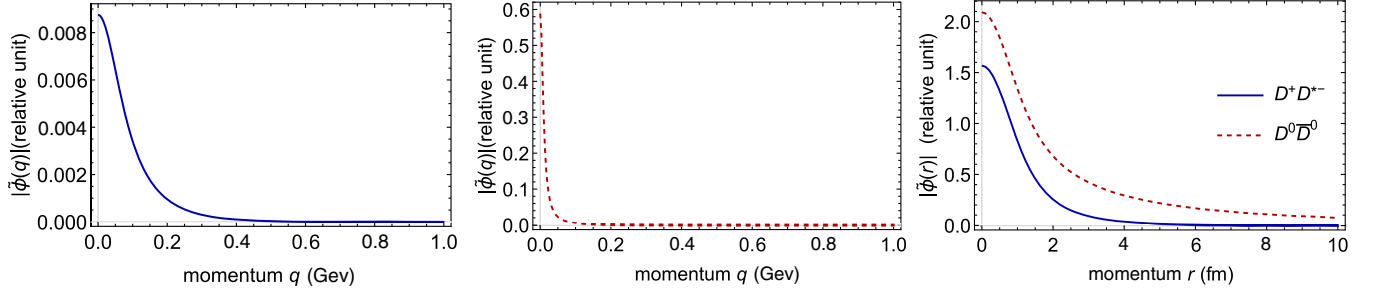


FIG. 6. The complex scaled wave function $\tilde{\phi}_l(\mathbf{q}) = \phi_l(\mathbf{q}e^{-i\theta})$ solved in Eq. (22). The first two graphs stand for the $D^0\bar{D}^{*0}$ (red dashed curve), $D^\pm\bar{D}^{*\mp}$ (blue solid curve) channels, respectively. The third graph shows the complex scaled wave function $\tilde{\phi}_l(\mathbf{r}) = \phi_l(\mathbf{r}e^{-i\theta})$ in coordinate space.

The contact terms can be written as a matrix

$$V_{ct} = \begin{bmatrix} V_{D^+D^{*0}} & V_{D^+D^{*0} \rightarrow D^0D^{*+}} \\ V_{D^0D^{*+} \rightarrow D^+D^{*0}} & V_{D^0D^{*+}} \end{bmatrix}, \quad (34)$$

which are related to

$$\begin{aligned} V_{D^+D^{*0}} &= V_{D^0D^{*+}} = \frac{1}{2}(V_{I=1} + V_{I=0}), \\ V_{D^+D^{*0} \rightarrow D^0D^{*+}} &= \frac{1}{2}(V_{I=1} - V_{I=0}), \end{aligned} \quad (35)$$

where $V_{I=0}$ and $V_{I=1}$ stand for the LO LECs of the $I = 0$ and $I = 1$ channels, respectively.

Since there are two undetermined LECs, we can no longer give a prediction of the width. But we find the result is hardly sensitive to $V_{I=1}$, which implies the state is dominated by the $I = 0$ channel. According to the quark model estimation, $V_{I=1} \approx 20 \text{ GeV}^{-2}$. Then $V_{I=0}$ is fixed to be -25.3 GeV^{-2} , which is in accordance with the simple calculation in Sec. IV A. Now the width is nearly doubled and rises up to around 78 keV. It is mainly a result of the variation of mass parameters, which increases the phase space, rather than the result of isospin breaking.

C. Possible bound states in the $D\bar{D}^*$ system

Then we turn to the $D\bar{D}^*$ system, which is related to the $\chi_{c1}(3872)$. With the exact isospin symmetry, the OPE potentials are exactly the same as their partners in the DD^* system due to their positive G parity (see Table I). The only difference is the LECs in the contact Lagrangians. As we can see from Fig. 5, the width of the $\chi_{c1}(3872)$ is of the order of 10 keV assuming its decay is dominated by the $D\bar{D}\pi$ decay channel.

However, the isospin breaking effect is significant for the $\chi_{c1}(3872)$, since the mass difference between the $D^0\bar{D}^{*0}$ and $D^+\bar{D}^{*-}$ is up to 8 MeV. The decay mode of the charged pions and D mesons is kinematically forbidden. Thus the only possible on-shell pion is in the $D^0\bar{D}^{*0}$ channel.

With the LECs in Table II, we derive $V_{I=0} = 2\tilde{D}_a + 6\tilde{E}_a \approx -47 \text{ GeV}^{-2}$ and $V_{I=1} = 2\tilde{D}_a - 2\tilde{E}_a \approx -2 \text{ GeV}^{-2}$ from the resonance saturation model. The pole position is determined mainly by the $V_{I=0}$, but $V_{I=1}$ has a considerable contribution, implying a large isospin breaking compared with the T_{cc}^+ . Figure 6 shows the complex scaled wave function with $V_{I=0} = -30 \text{ GeV}^{-2}$, $V_{I=1} = 5 \text{ GeV}^{-2}$. The pole lies at $E = (-0.114 - 0.017i) \text{ MeV}$. It is mainly a bound state of $D^0\bar{D}^{*0}$. Figure 7 shows the corresponding result of CSM. The binding energy with respect to the $D^0\bar{D}^{*0}$ threshold is so small that the distribution of the wave function in momentum space is quite narrow in momentum

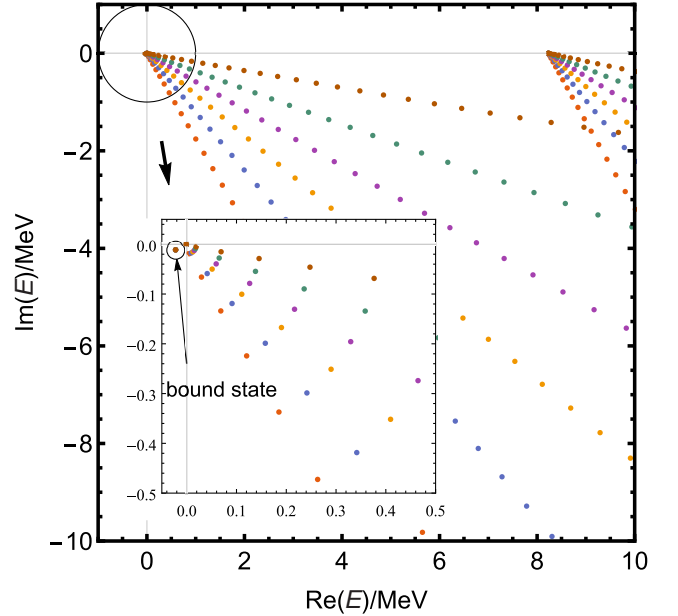


FIG. 7. Positions of the bound state corresponding to the $\chi_{c1}(3872)$ found in the $D\bar{D}^*$ system. Dots with different colors represent the continuum states with the rotation angle $\theta = 5^\circ, 10^\circ, 15^\circ, 20^\circ, 25^\circ, 30^\circ$. The dots on the left represent the $D^0\bar{D}^{*0}$ continuum and the dots on the right represent the $D^+\bar{D}^{*-}$ continuum. The lines always start from one of the thresholds. The unstable bound state lies below the line of the continuum states and stays static when θ varies.

TABLE IV. Variation of the pole position $E = \delta m - i\Gamma/2$ (MeV) with respect to the $D^0 D^{*+}$ threshold with the contact terms. It is sensitive to $V_{I=0}$ rather than $V_{I=1}$, which implies the pole is related to the $I = 0$ state with a small isospin breaking effect. $V_{I=0}$ refers to C_s in Table III.

		$V_{I=0}$ (GeV ⁻²)			
		-26	-25	-24	-23
$V_{I=1}$ (GeV ⁻²)	-10	-0.537-0.039i	-0.348-0.040i	-0.190-0.041i	-0.075-0.035i
	0	-0.515-0.039i	-0.325-0.040i	-0.166-0.040i	-0.054-0.033i
	10	-0.502-0.039i	-0.311-0.040i	-0.153-0.040i	-0.043-0.031i
	20	-0.494-0.038i	-0.303-0.039i	-0.145-0.040i	-0.037-0.030i
	30	-0.488-0.038i	-0.297-0.039i	-0.139-0.039i	-0.032-0.029i
	40	-0.484-0.038i	-0.292-0.039i	-0.135-0.039i	-0.029-0.029i

space and quite wide in coordinate space. The wave functions seem comparable at small r , but the wave function of $D^0 \bar{D}^{*0}$ declines slowly as r increases. The $D^0 \bar{D}^{*0}$ channel takes up 94% of the state, $D \bar{D} \pi$ takes up 1% and $D^\pm \bar{D}^{*\mp}$ takes up the rest. If the state is closer to the threshold, then the isospin breaking will become larger.

The probability of three-body components is calculated by [58,59]

$$P_{3b} = \frac{(\phi | -\frac{\partial V}{\partial E} | \phi)}{(\phi | \phi)}, \quad (36)$$

where the inner product is defined by the so-called c product

$$(\phi | \phi) = \int \phi(\mathbf{p})^2 \frac{d^3 \mathbf{p}}{(2\pi)^3}. \quad (37)$$

The wave function takes the place of its complex conjugate compared with the normal inner product.

When $V_{I=0}$ and $V_{I=1}$ vary, we find the width Γ is always of the order of 10 keV, even smaller than the width of the T_{cc}^+ , as shown in Table V. So if we assume the $D^0 D^0 \pi^0$ and $D^0 D^{*0}$ as the dominant decay channels, the width of the $\chi_{c1}(3872)$ will be only of the order of 10 keV. Although this width looks too narrow, it is still within a standard deviation compared with the result of the pole search in Ref. [4]. The binding is so loose that the bound state may disappear if the potential is a little less attractive. The bound state pole can move above the $D^0 \bar{D}^{*0}$ threshold with some specific sets of parameters, but we still recognize it as a (quasi)bound state because it locates at the physical Riemann sheet.

By analogy with the nucleon antinucleon ($N\bar{N}$) annihilation effects, we can introduce a complex \tilde{C}_s , according to the optical theorem, to take into account the inelastic channels, including the hidden-charm final states. This is based on the consideration that these processes usually include final states with large momenta and are related to the short-ranged physics. Though we have little knowledge of how large the imaginary parts should be, we let them be of the same order of magnitude of their real parts, as we can see in the nucleon systems [60]. Due to the unitarity

constraints, the imaginary part of the Feynman amplitudes satisfies $\text{Im} \mathcal{M} > 0$. Then we demand $\text{Im} \tilde{C}_s < 0$. One can refer to Ref. [61] for an example of this kind of complex potential.

If we introduce the imaginary parts to the contact terms, then the width of the $\chi_{c1}(3872)$ will increase rapidly. For example, the pole will move to 0.10-0.39i MeV if we set $V_{I=0} = -30 - 3i$ GeV⁻² and $V_{I=1} = 5$ GeV⁻². The partial width of the $\chi_{c1}(3872)$ decaying to the $D \bar{D} \pi$ final states is small due to the limited phase space. If the total width is much larger than the order of magnitude of 10 keV, then it cannot be explained by the $D \bar{D} \pi$ decay, and other decay channels including the hidden-charm decay modes are important.

D. Corrections from heavy meson kinetic energies

In the framework of HMChEFT, the kinetic energies of heavy mesons are ignored. It is a reasonable approximation since the kinetic energies are small compared to the meson masses. However, the characteristic energy considered here is $\delta - m_\pi \approx 3$ MeV, and the kinetic energy terms have a considerable contribution to the width of the state.

To evaluate the corrections from heavy meson kinetic energies, we revise Eq. (29) to its relativistic form. A relativistic kinetic energy term is introduced²

$$\delta_i \longrightarrow m_D + m_{D^*} - \sqrt{p_1^2 + m_{D,i}^2} - \sqrt{p_3^2 + m_{D,f}^2}. \quad (38)$$

A comparison of results with or without isospin conservation and $1/m_D$ corrections is summarized in Table VI. According to Tables IV and V, the widths of the T_{cc}^+ and $\chi_{c1}(3872)$ are stable as the LECs vary, especially when we keep the binding energy fixed, so we only list the widths in Table VI. The binding energies are set to 360 and 100 keV for the T_{cc}^+ and $\chi_{c1}(3872)$, respectively. We find the width drops by half when the kinetic energies included.

² Apart from the Lagrangians and the Feynman diagrams, Eq. (27) should be revised because of the normalization factor $-\prod_i \frac{1}{\sqrt{2M_i}} \rightarrow -\prod_i \frac{1}{\sqrt{2E_i}}$.

TABLE V. The variation of the pole position $E = \delta m - i\Gamma/2$ (MeV) corresponding to the $D^0\bar{D}^{*0}$ with the contact terms. It is sensitive to both $V_{I=0}$ and $V_{I=1}$, which implies the isospin breaking effect is significant. The symbols are the same as in Table IV.

	$V_{I=1}$ (GeV ⁻²)		
	-5	5	15
$V_{I=0}$			
(GeV ⁻²)			
-36	-1.591-0.014i	-1.498-0.014i	-1.430-0.014i
-34	-0.995-0.017i	-0.902-0.017i	-0.834-0.017i
-32	-0.517-0.020i	-0.431-0.019i	-0.370-0.019i
-30	-0.178-0.019i	-0.114-0.017i	-0.074-0.016i
-28	-0.008-0.012i	0.015-0.009i	...

TABLE VI. The width (unit: keV) of the pole found in the DD^* and $D\bar{D}^*$ systems. The isospin conserved condition in the $D\bar{D}^*$ system is not included since the isospin breaking effect is large.

	Isospin conserving	Isospin breaking	Isospin breaking and $1/m_D$ corrections
DD^*	42	78	36
$D\bar{D}^*$...	34	15

This result is consistent with Ref. [45]. Additionally, we find the relativistic form and the nonrelativistic form of the kinetic energy show no difference.

The contribution of the D^* width is not included here. Since the analytical form of the D^* self-energy is regulator dependent and may involve an extra parameter, we will include this important aspect of the three-body effect in several different ways and present the results in a separate section.

E. Effects of the D^* width

Inserting Eq. (18) into Eq. (25), we make a full calculation involving the effect of the D^* width. The isospin breaking effects in Secs. IV B and IV C, together with the heavy meson recoil corrections in Sec. IV D, are included. The numerical results are stable with different complex scaling angles. The results are shown in Table VII. The first column is adapted from Table VI. The second column includes the effect of the D^* width but omit heavy meson kinetic terms in the D^* width and the OPE potential. The third column includes the effect of the D^* width and the heavy meson recoil corrections. Similar to Table VI, only widths are listed.

For the T_{cc}^+ , the influence of the D^* width is of the same order of magnitude as the OPE potential, which is consistent with the naive intuition from Fig. 1. But for $\chi_{c1}(3872)$, the effect of the D^* width is relatively small because of the small phase space. The only allowed decay is $D^{*0} \rightarrow D^0\pi^0$.

TABLE VII. The widths of the T_{cc}^+ and $\chi_{c1}(3872)$ when the effect of the D^* width is included (unit: keV).

	Without D^* width	With D^* width	With D^* width and $1/m_D$ corrections
T_{cc}^+	78	138	79
$\chi_{c1}(3872)$	34	66	45

The inclusion of the D^* width nearly doubles the widths, indicating the two aspects of the three-body effect, namely the D^* width and the three-body cut in the OPE potential, are of similar significance. It is natural since they follow the same mechanism in Fig. 1. Consistent with Ref. [45], the width declines significantly once the corrections of the heavy meson kinetic terms are included. This is because the two-body phase space of the D^* decay is related to $E - \mathbf{p}^2/2\mu$, as shown in Eq. (19). It is sensitive to the heavy meson recoil energy since the phase space ($E \sim m_{D^*} - m_D - m_\pi$) is very small. If we artificially increase the mass difference of D and D^* , then the recoil corrections will become negligible.

We further investigate the systematic errors of omitting the real part of the D^* self-energy. The real part is not constrained by the unitarity, so we calculate the self-energy using the HMChEFT and $\overline{\text{MS}}$ scheme. Equation (25) becomes

$$E\phi_l(p) = \left[\frac{p^2}{2\mu} + \frac{1}{2}(\Sigma(E) - \Sigma(E_0)) \right] \phi_l(p) + \int \frac{p'^2 dp'}{(2\pi)^3} V_{l,l'}(p, p') \phi_{l'}(p'), \quad (39)$$

where the subtraction of $\Sigma(E_0)$ is the result of the on-shell renormalization. Here E_0 corresponds to the “physical” pole mass of D^* .³ If we choose the threshold $m_{th} = m_{D^*} - \frac{i}{2}\Gamma_{D^*} + m_D$, then $E_0 = 0$. Another approximate way is ignoring the width and choosing a real-valued E_0 . Then we have $m_{th} = m_{D^*} + m_D$ and $E_0 = 0$, and only the real part of the self-energy $\text{Re}\Sigma(E_0)$ is subtracted. Note that E_0 is the energy with respect to the DD^* threshold.

The self-energies read

$$\begin{aligned} \Sigma_{D^{*+}}(E) &= 2\Sigma(E_{D^*} - m_{D^0}, m_{\pi^+}) + \Sigma(E_{D^*} - m_{D^+}, m_{\pi^0}), \\ \Sigma_{D^{*0}}(E) &= 2\Sigma(E_{D^*} - m_{D^+}, m_{\pi^-}) + \Sigma(E_{D^*} - m_{D^0}, m_{\pi^0}), \end{aligned} \quad (40)$$

³The “physical” and “bare” mass and width are related by $m_0 - \frac{i}{2}\Gamma_0 + \frac{1}{2}\Sigma(E_0) = E_0$. The “bare” Γ_0 arises from the decays other than the decay to $D\pi$ channels, and its energy dependence can be ignored.

where E_{D^*} is the energy of D^* in its rest frame, and

$$\Sigma(\omega, m) = -\frac{g^2}{2f_\pi^2} J_{22}^a(m, \omega). \quad (41)$$

Its imaginary part gives Eq. (18) under the heavy quark limit $\frac{m_D}{m_{D^*}} \rightarrow 1$. $\Sigma(E_{D^*} - m_{D^+}, m_{\pi^-})$ is real valued when E_{D^*} is real valued, since D^{*0} decaying to $D^+\pi^-$ is kinetically forbidden. But when E_{D^*} is complex valued, it does affect the imaginary part of the pole position.

The definition of the loop integral J_{22}^a can be found in Ref. [62],

$$J_{22}^a(m, \omega) = i \int \frac{d^4 l}{(2\pi)^4} \frac{-\frac{1}{3} \mathbf{l}^2}{(v \cdot l + \omega + i\epsilon)(l^2 - m^2 + i\epsilon)}. \quad (42)$$

Considering the complete form of self-energies, as well as the recoil corrections for E_{D^*} and OPE, we find

$$\Gamma_{T_{cc}^+} = 72 \text{ keV}, \quad \Gamma_{\chi_{c1}(3872)} = 50 \text{ keV}, \quad (43)$$

which shows little difference with the last column in Table VII.

V. SUMMARY

In summary, we perform a CSM calculation with the LO chiral interaction involving three-body effects in S-wave DD^* and $D\bar{D}^*$ systems, to investigate the molecular properties of T_{cc}^+ and $\chi_{c1}(3872)$. We have included the isospin breaking, the recoil correction, the effect of D^* width and quantitatively analyzed their influence. The widths of the above two bound states are derived naturally via the three-body effect.

In our calculation, the complex scaling method turns out to be a useful tool to deal with the singularity in the potential. And it helps solve the resonances and unstable bound states which are beyond the reach of the traditional Schrödinger equation. With a non-Hermitian Hamiltonian, the eigenenergy gains a negative imaginary part, indicating that the state decays.

At the very heart of this work is the three-body effect. The accidental comparability between the pion mass and the $D^* - D$ mass splitting makes on-shell intermediate three-body state very important. We have proposed a revised OPE potential with pions treated relativistically, to satisfy the three-body unitarity. With the energy of the exchanged pion retained, the OPE potential is dependent on the $DD^*/D\bar{D}^*$ center-of-mass energy, which is somehow equivalent to a coupled-channel analysis involving both the three-body $DD\pi$ channel and two-body DD^* channel. The revised OPE potential introduces a unitary cut at the $DD\pi$ three-body threshold. Its energy dependence gives the ratio of three-body components in T_{cc}^+ and $\chi_{c1}(3872)$.

For the DD^* system, we find only one pole in the first Riemann sheet with respect to the DD^* threshold, corresponding to the T_{cc}^+ . It is a DD^* bound state and $DD\pi$ resonance. Its width arises from the decay to $DD\pi$, which has been included nonperturbatively. The width gradually goes to zero when the pole moves towards the $DD\pi$ threshold. But if we fix the real part of the pole position (binding energy) to the experiment value, the imaginary part (width) is nearly independent of the cutoff or the contact term of the $I = 1$ channel, which allows us to make a powerful prediction on the width based on the binding energy. After considering the isospin breaking effect, the recoil correction and the D^* width, we find the width of the T_{cc}^+ to be 72 keV.

As for the $\chi_{c1}(3872)$, the isospin symmetry breaking effect is significant, so there are too many independent LECs to make a prediction. But using estimations of the LECs from the quark model, we do find a pole corresponding to the $\chi_{c1}(3872)$. Considering the recoil correction and the D^* width, we find the width of the $\chi_{c1}(3872)$ to be 50 keV, which is much smaller than the experimental value obtained either with the Breit-Wigner or Flatté models, but is within one standard deviation of the pole search. Because the phase space of the open-charm decay of the $\chi_{c1}(3872)$ is so limited, the partial decay width to $D\bar{D}\pi$ ought to be small. The possible $c\bar{c}$ components may explain the deviation of widths. The hidden-charm decay and electromagnetic decay in theoretic calculations, together with more precise measurements in experiments, are called for in further study.

Furthermore, we investigate the influence of the recoil correction and D^* width, which is important in the three-body kinetics. We find the recoil correction notably reduces the width of T_{cc}^+ and $\chi_{c1}(3872)$. It is mainly because the small phase space amplifies the effect of recoil corrections, which is supposed to be suppressed by $1/m_{D^{(*)}}$. Then we introduce a Schrödinger equation for unstable particles to involve the D^* width. We find the widths of the T_{cc}^+ and $\chi_{c1}(3872)$ are nearly doubled when considering the D^* width, and are significantly reduced when considering the heavy meson kinetic energy corrections. This formalism is equivalent to the Lippmann-Schwinger equation for unstable particles and can be extended to other systems where the width of particles are non-negligible.

Besides, we find the two-pion-exchange potentials in HMChEFT violate the three-body unitarity and might lead to a potential with a positive imaginary part in some cases. This implies they should not be directly included in the iterative equations before a proper treatment satisfying the unitarity has been done, which needs further investigations.

ACKNOWLEDGMENTS

This research is supported by the National Science Foundation of China under Grants No. 11975033,

No. 12070131001, and No. 12147168. The authors thank G. J. Wang for helpful discussions.

APPENDIX A: THE EQUIVALENCE FOR THE SCHRÖDINGER EQUATION AND THE LIPPMANN-SCHWINGER EQUATION FOR UNSTABLE PARTICLES

Equation (26) can be written as $T = V + VGT$, where the Green's function or propagator $G = \frac{1}{E - p^2/2\mu + i\Gamma(E)/2}$ includes the width of the unstable particle. Then the poles of the T matrix are searched for via the zeros of the Fredholm determinant of $(1 - VG)$. $\text{Det}[1 - VG] = 0$ implies $(1 - VG)$ has at least one eigenvalue equal to 0. Let ϕ denote the corresponding eigenvector, namely $(1 - VG)\phi = 0$. Note that the Green's function is invertible $G = (E - H_0)^{-1}$, where $H_0 = p^2/2\mu - i\Gamma(E)/2$. Then one can derive $(G^{-1} - V)(G\phi) = 0$ or $(E - H_0 - V)\tilde{\phi} = 0$, where $\tilde{\phi} = G\phi$. It is exactly Eq. (25).

In fact, in quantum mechanics, the propagator in the LS equation comes from the H_0 in the interaction picture, which corresponds to the kinetic terms in the Schrödinger equation. This simply gives the equivalence of Eqs. (26) and (25).

APPENDIX B: ESTIMATIONS OF LECs

We use two models to estimate the LECs in the $DD^*(\bar{D}^*)$ system in Table II. In the single-channel case (Sec. IV A), there is only one independent LEC and it can be determined by the mass of T_{cc}^+ . The fitted value is consistent with the estimated value. In coupled-channel cases, the number of LECs exceeds the number of observables. Therefore, we use the estimated LECs to give predictions. In principle, the LECs depend on the cutoff Λ . We fix the cutoff Λ and let the LECs vary around the estimated values.

1. Model I

In line with Ref. [55], the resonance saturation model is performed to determine the LECs. In this model, the contact interactions arise from meson changes including the ρ , ω , σ , and other scalar or axial-vector mesons. The masses of mesons are relatively large, which results in a short-range interaction. We take the following substitution in propagators to generate contact interactions

$$q^2 \longrightarrow 0. \quad (\text{B1})$$

In the one-boson-exchange model, the Lagrangian for the vector mesons reads

$$\mathcal{L}_{HHV} = -i\beta \langle H v_\mu \rho^\mu \bar{H} \rangle + i\lambda \langle H \sigma_{\mu\nu} F^{\mu\nu} \bar{H} \rangle, \quad (\text{B2})$$

where $F^{\mu\nu}$ stands for the field-strength tensor $F^{\mu\nu} = \partial_\mu \rho_\nu - \partial_\nu \rho_\mu - [\rho_\mu, \rho_\nu]$. $\rho_\mu = \frac{i g_\rho}{\sqrt{2}} \hat{\rho}_\mu$ includes ρ and ω mesons under $U(2)$ symmetry

$$\hat{\rho}^\mu = \begin{pmatrix} \frac{\rho_0}{\sqrt{2}} + \frac{\omega}{\sqrt{2}} & \rho^+ \\ \rho^- & -\frac{\rho_0}{\sqrt{2}} + \frac{\omega}{\sqrt{2}} \end{pmatrix}^\mu. \quad (\text{B3})$$

The Lagrangians for the scalar and axial-vector mesons read

$$\begin{aligned} \mathcal{L}_{HHS} &= g_{HHS} \langle H S \bar{H} \rangle, \\ \mathcal{L}_{HHA_v} &= g_{HHA_v} \langle H \gamma_\mu \gamma_5 A_v^\mu \bar{H} \rangle, \end{aligned} \quad (\text{B4})$$

where S is the scalar field operator, and A_v is the axial-vector field operator.

They contribute to the D_a and E_a terms according to the Lorentz structure and isospin. For the DD^* system,

$$\begin{aligned} D_a &= -\frac{\beta^2 g_v^2}{8m_\omega^2} + \frac{g_s^2}{2m_\sigma^2} + \frac{g_{s0}^2}{12m_{f_0}^2}, & E_a &= -\frac{\beta^2 g_v^2}{8m_\rho^2} - \frac{g_{s0}^2}{4m_{a_0}^2}, \\ D_b &= \frac{g_{HHA}^2}{8m_{a_1}^2}, & E_b &= \frac{g_{HHA}^2}{8m_{f_1}^2}, \end{aligned} \quad (\text{B5})$$

where βg_v , g_s , g_{s0} , g_{HHA} are coupling constants for $\rho(\omega)$, σ and $f_0(a_0)$, respectively. We take $\beta = 0.9$, $g_v = 5.8$, $g_s = 0.76$, and $g_{s0} = \sqrt{3}g_s$ [63,64].

For the $D\bar{D}^*$ system, the $\omega/a_0/a_1$ exchange changes the sign,

$$\begin{aligned} \tilde{D}_a &= -\frac{\beta^2 g_v^2}{8m_\omega^2} - \frac{g_s^2}{2m_\sigma^2} - \frac{g_{s0}^2}{12m_{f_0}^2}, & \tilde{E}_a &= -\frac{\beta^2 g_v^2}{8m_\rho^2} + \frac{g_{s0}^2}{4m_{a_0}^2}, \\ \tilde{D}_b &= \frac{g_{HHA}^2}{8m_{a_1}^2}, & \tilde{E}_b &= \frac{g_{HHA}^2}{8m_{f_1}^2}. \end{aligned} \quad (\text{B6})$$

Assuming LECs are saturated by the resonances below 800 MeV, we estimated the LECs including the contributions of the ρ , ω , and σ mesons,

$$\begin{aligned} D_a &\approx -4.4 \text{ GeV}^{-2}, & E_a &\approx -5.7 \text{ GeV}^{-2}, \\ \tilde{D}_a &\approx -6.7 \text{ GeV}^{-2}, & \tilde{E}_a &\approx -5.7 \text{ GeV}^{-2}. \end{aligned} \quad (\text{B7})$$

2. Model II

In model II, we estimate LECs using quark-level Lagrangians. In Refs. [10,57], the interactions between quarks are induced by the exchange of the fictitious scalar field \mathcal{S} and axial-vector field \mathcal{A} ,

$$\mathcal{L} = g_s \bar{q} \mathcal{S} q + g_a \bar{q} \gamma_\mu \gamma_5 \mathcal{A}^\mu q. \quad (\text{B8})$$

The scalar field \mathcal{S} and axial-vector field \mathcal{A} are assumed to form a $SU(3)$ octet in flavor space. In $SU(2)$ case, they can be decomposed into isospin triplets and singlets,

$$\begin{aligned}\mathcal{S} &= \mathcal{S}_3 \tau^i + \frac{1}{\sqrt{3}} \mathcal{S}_1 \tau^0, \\ \mathcal{A}^\mu &= \mathcal{A}_3^\mu \tau^i + \frac{1}{\sqrt{3}} \mathcal{A}_1^\mu \tau^0,\end{aligned}\quad (\text{B9})$$

where τ^0 denotes the identity matrix. The $\sqrt{3}$ factor arises from the Gell-Mann matrix λ_8 .

Again the exchanged particles are assumed to be heavy. Then we obtain the contact interactions between the light quarks,

$$\begin{aligned}V_{qq} &= c_s(1 + 3\tau_1 \cdot \tau_2) + c_t(1 + 3\tau_1 \cdot \tau_2)\sigma_1 \cdot \sigma_2, \\ V_{q\bar{q}} &= \tilde{c}_s(1 - 3\tau_1 \cdot \tau_2) + \tilde{c}_t(1 - 3\tau_1 \cdot \tau_2)\sigma_1 \cdot \sigma_2.\end{aligned}\quad (\text{B10})$$

The coefficients c_s and c_t stand for the central potential and the spin-spin interaction, respectively. They are to be determined in the $NN(\bar{N})$ systems.

At the hadron level, the potential can be written in the form of the hadron spin and isospin,

$$\begin{aligned}V_{DD^*} &= c_s(1 + 3\tau_1 \cdot \tau_2), \\ V_{D\bar{D}^*} &= \tilde{c}_s(1 - 3\tau_1 \cdot \tau_2), \\ V_{NN} &= c_s(9 + 3\tau_1 \cdot \tau_2) + c_t\left(1 + \frac{25}{3}\tau_1 \cdot \tau_2\right)\sigma_1 \cdot \sigma_2, \\ V_{N\bar{N}} &= c_s(9 - 3\tau_1 \cdot \tau_2) + c_t\left(1 - \frac{25}{3}\tau_1 \cdot \tau_2\right)\sigma_1 \cdot \sigma_2.\end{aligned}\quad (\text{B11})$$

In Ref. [10], the qq interactions are determined by the experimental mass of the P_c states,

$$c_s = 3.9 \text{ GeV}^{-2}, \quad c_t = -0.95 \text{ GeV}^{-2}.\quad (\text{B12})$$

In Ref. [57], the $q\bar{q}$ interactions are determined by the scattering of $N\bar{N}$,

$$\tilde{c}_s = -8.1 \text{ GeV}^{-2}, \quad \tilde{c}_t = 0.65 \text{ GeV}^{-2}.\quad (\text{B13})$$

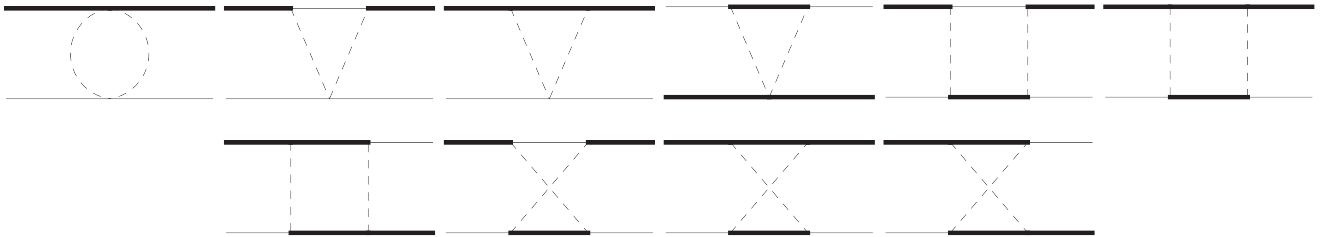


FIG. 8. TPE diagrams. The thick, thin, and dashed lines represent D^* , D , π , respectively. The second, fifth, and eighth diagrams have imaginary parts corresponding to on-shell intermediate states.

APPENDIX C: TWO-PION EXCHANGE POTENTIALS

The imaginary part of the TPE potential naturally shows up in the loop integral. We include the TPE contributions and investigate its influence on the width of the T_{cc}^+ and $\chi_{c1}(3872)$. Its influence on the binding energy can be compensated by the adjustment of LECs.

Since we calculate the TPE potentials under HMCheFT, namely all $1/M$ corrections are dropped, the kinetic energy corrections in OPE are not considered.

The TPE diagrams are shown in Fig. 8. The specific expressions can be found in Refs. [55,62]. For the fifth diagram, in which the intermediate DD^* are on shell, a direct calculation in the heavy meson scheme leads to an infrared divergence, or a $m_{D^{(*)}}/p$ enhancement if we retain the $1/m_D$ corrections. It violates the naive power counting rule, and hence needs to be subtracted according to Weinberg's power counting scheme. Only 2PI parts of the diagrams contribute to the effective potential. In previous subtraction schemes, however, the fifth diagram has a large imaginary part after subtraction, which violates the unitarity condition. To avoid the potential ambiguity of being unphysical, we drop the fifth diagram instead of subtracting its two-particle-reducible (2PR) part. For other planar box diagrams, we subtract the 2PR parts in line with the scheme in the appendix of Ref. [65].

Figure 9 shows the TPE potential versus the transferred momentum q . In S-wave cases, it is equivalent to replace p with q , so we simply plot the potential as a function of q . There is a pole on the real axis at $|q| = 2\sqrt{\delta^2 - m_\pi^2}$. We avoid the pole in the integral by rotating in the complex momentum plane. The imaginary part arises from the cut in Fig. 10. For the subdiagrams G_i in Fig. 10, we use M_{G_i} to denote their amplitudes. The unitarity is guaranteed since the imaginary part (discontinuity) of the forward scattering amplitude is proportional to the total cross section

$$\text{disc } M \propto \left(\sum_{G_i} M_{G_i}\right) \left(\sum_{G_i} M_{G_i}\right)^* > 0.\quad (\text{C1})$$

However, in a perturbative calculation, all these diagrams are not included. For instance, up to $\mathcal{O}(p^2)$, we include only $|M_{G_1}|^2$ (the OPE and the D^* width) and $M_{G_1}^* M_{G_2}$ (the

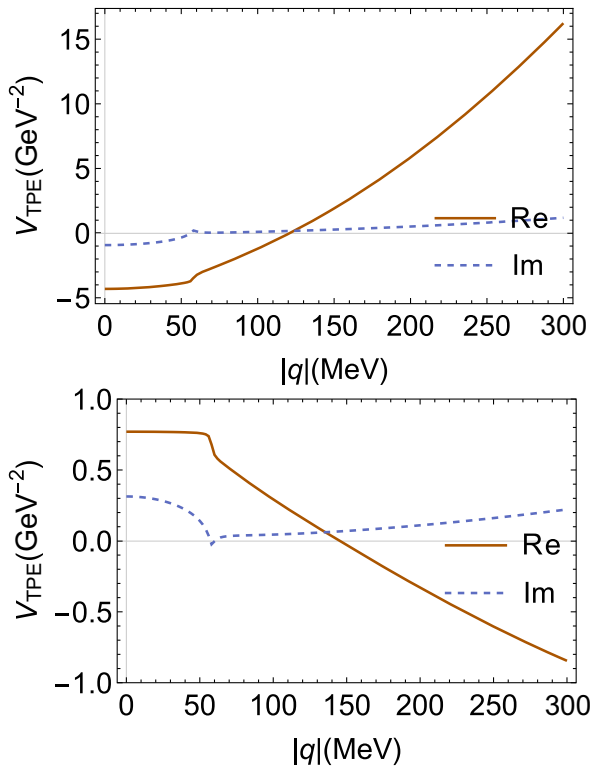


FIG. 9. The TPE potentials $V_{\text{TPE}}(qe^{-i\theta})$ for $I = 0$ (left) and $I = 1$ (right) DD^* systems when $\theta = 1^\circ$. There is a pole near $|q| = 60$ MeV corresponding to the on-shell pion if θ goes to zero.

left diagram in Fig. 10). $|M_{G_2}|^2$ is not included since it is of higher order. So the unitarity is not guaranteed, which may result in a positive imaginary part of the potential. In Weinberg's scheme, the 2PR part of the right diagram in Fig. 10 must be subtracted, but the previous subtraction scheme leads to an unphysically large imaginary part. So we exclude the corresponding diagram to protect unitarity.

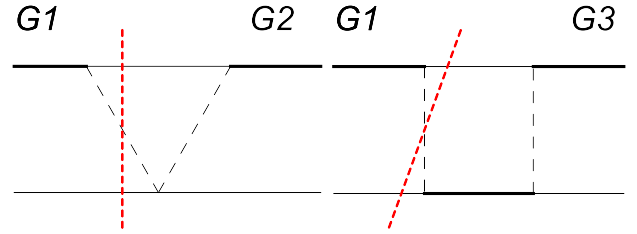


FIG. 10. Examples of on-shell intermediate states in TPE.

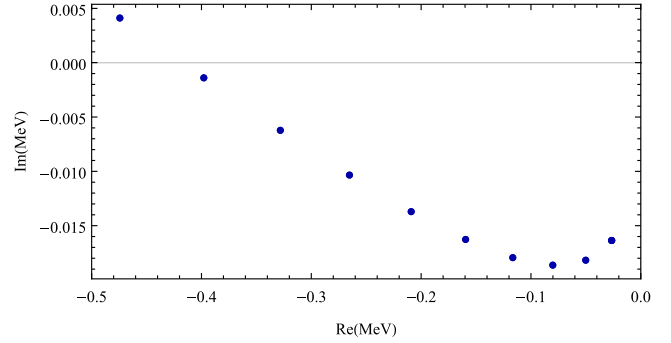


FIG. 11. Bound states in the $I = 0$ S -wave DD^* system with the OPE, TPE, and contact terms. When we shift C_s from -41 to -32 GeV^{-2} , the pole moves in the positive real axis direction.

For similar reasons, one-loop corrections to the OPE potential are not included.

Figure 11 shows the pole position of the T_{cc}^+ in $I = 0$ channel as C_s varies from -41 to -32 GeV^{-2} . It seems the width declines and the pole can move to the upper half plane. But it is a result of the breaking of the unitarity, which is unphysical. In the framework of HMChEFT, one must be careful about the TPE when dealing with widths.

-
- [1] R. Aaij *et al.* (LHCb Collaboration), Observation of an exotic narrow doubly charmed tetraquark, *Nat. Phys.* **18**, 751 (2022).
 - [2] R. Aaij *et al.* (LHCb Collaboration), Study of the doubly charmed tetraquark T_{cc}^+ , *Nat. Commun.* **13**, 3351 (2022).
 - [3] S.K. Choi *et al.* (Belle Collaboration), Observation of a narrow charmonium-like state in exclusive $B^\pm \rightarrow K^\pm \pi^+ \pi^- J/\psi$ decays, *Phys. Rev. Lett.* **91**, 262001 (2003).
 - [4] R. Aaij *et al.* (LHCb Collaboration), Study of the lineshape of the $\chi_{c1}(3872)$ state, *Phys. Rev. D* **102**, 092005 (2020).
 - [5] R.L. Workman *et al.* (Particle Data Group), Review of particle physics, *Prog. Theor. Exp. Phys.* **2022**, 083C01 (2022).
 - [6] A. V. Manohar and M. B. Wise, Exotic QQqq states in QCD, *Nucl. Phys.* **B399**, 17 (1993).
 - [7] D. Janc and M. Rosina, The $T_{cc} = DD^*$ molecular state, *Few Body Syst.* **35**, 175 (2004).
 - [8] S. Ohkoda, Y. Yamaguchi, S. Yasui, K. Sudoh, and A. Hosaka, Exotic mesons with double charm and bottom flavor, *Phys. Rev. D* **86**, 034019 (2012).
 - [9] R. Chen, Q. Huang, X. Liu, and S.-L. Zhu, Predicting another doubly charmed molecular resonance $T_{cc}^{\prime+}(3876)$, *Phys. Rev. D* **104**, 114042 (2021).
 - [10] K. Chen, R. Chen, L. Meng, B. Wang, and S.-L. Zhu, Systematics of the heavy flavor hadronic molecules, *Eur. Phys. J. C* **82**, 581 (2022).

- [11] K. Chen, B. Wang, and S.-L. Zhu, Heavy flavor molecular states with strangeness, *Phys. Rev. D* **105**, 096004 (2022).
- [12] X.-K. Dong, F.-K. Guo, and B.-S. Zou, A survey of heavy-heavy hadronic molecules, *Commun. Theor. Phys.* **73**, 125201 (2021).
- [13] C. Deng and S.-L. Zhu, T_{cc}^+ and its partners, *Phys. Rev. D* **105**, 054015 (2022).
- [14] A. Feijoo, W.H. Liang, and E. Oset, $D^0 D^0 \pi^+$ mass distribution in the production of the T_{cc} exotic state, *Phys. Rev. D* **104**, 114015 (2021).
- [15] L. R. Dai, R. Molina, and E. Oset, Prediction of new T_{cc} states of $D^* D^*$ and $D_s^* D^*$ molecular nature, *Phys. Rev. D* **105**, 016029 (2022).
- [16] C.-R. Deng and S.-L. Zhu, Decoding the double heavy tetraquark state T_{cc}^+ , *Sci. Bull.* **67**, 1522 (2022).
- [17] M. Albaladejo, T_{cc}^+ coupled channel analysis and predictions, *Phys. Lett. B* **829**, 137052 (2022).
- [18] J. I. Ballot and J. M. Richard, Four quark states in additive potentials, *Phys. Lett.* **123B**, 449 (1983).
- [19] S. Zouzou, B. Silvestre-Brac, C. Gignoux, and J. M. Richard, Four quark bound states, *Z. Phys. C* **30**, 457 (1986).
- [20] Y. Yang, C. Deng, J. Ping, and T. Goldman, S -wave $QQ\bar{q}\bar{q}$ state in the constituent quark model, *Phys. Rev. D* **80**, 114023 (2009).
- [21] A. V. Berezhnuy, A. K. Likhoded, and A. V. Luchinsky, Doubly heavy baryons at the LHC, *Phys. Rev. D* **98**, 113004 (2018).
- [22] G. Yang, J. Ping, and J. Segovia, Doubly-heavy tetraquarks, *Phys. Rev. D* **101**, 014001 (2020).
- [23] Y. Tan, W. Lu, and J. Ping, Systematics of $QQ\bar{q}\bar{q}$ in a chiral constituent quark model, *Eur. Phys. J. Plus* **135**, 716 (2020).
- [24] T. Guo, J. Li, J. Zhao, and L. He, Mass spectra of doubly heavy tetraquarks in an improved chromomagnetic interaction model, *Phys. Rev. D* **105**, 014021 (2022).
- [25] Q. Meng, M. Harada, E. Hiyama, A. Hosaka, and M. Oka, Doubly heavy tetraquark resonant states, *Phys. Lett. B* **824**, 136800 (2022).
- [26] M.-L. Du, W. Chen, X.-L. Chen, and S.-L. Zhu, Exotic $QQ\bar{q}\bar{q}$, $QQ\bar{q}\bar{s}$ and $QQ\bar{s}\bar{s}$ states, *Phys. Rev. D* **87**, 014003 (2013).
- [27] G. K. C. Cheung, C. E. Thomas, J. J. Dudek, and R. G. Edwards (Hadron Spectrum Collaboration), Tetraquark operators in lattice QCD and exotic flavour states in the charm sector, *J. High Energy Phys.* **11** (2017) 033.
- [28] P. Junnarkar, N. Mathur, and M. Padmanath, Study of doubly heavy tetraquarks in Lattice QCD, *Phys. Rev. D* **99**, 034507 (2019).
- [29] H.-X. Chen, W. Chen, X. Liu, and S.-L. Zhu, The hidden-charm pentaquark and tetraquark states, *Phys. Rep.* **639**, 1 (2016).
- [30] A. Esposito, A. Pilloni, and A. D. Polosa, Multiquark resonances, *Phys. Rep.* **668**, 1 (2017).
- [31] F.-K. Guo, C. Hanhart, U.-G. Meißner, Q. Wang, Q. Zhao, and B.-S. Zou, Hadronic molecules, *Rev. Mod. Phys.* **90**, 015004 (2018).
- [32] Y.-R. Liu, H.-X. Chen, W. Chen, X. Liu, and S.-L. Zhu, Pentaquark and tetraquark states, *Prog. Part. Nucl. Phys.* **107**, 237 (2019).
- [33] N. Brambilla, S. Eidelman, C. Hanhart, A. Nefediev, C.-P. Shen, C. E. Thomas, A. Vairo, and C.-Z. Yuan, The XYZ states: Experimental and theoretical status and perspectives, *Phys. Rep.* **873**, 1 (2020).
- [34] H.-X. Chen, W. Chen, X. Liu, Y.-R. Liu, and S.-L. Zhu, An updated review of the new hadron states, *Rep. Prog. Phys.* **86**, 026201 (2023).
- [35] S. Weinberg, Nuclear forces from chiral Lagrangians, *Phys. Lett. B* **251**, 288 (1990).
- [36] S. Weinberg, Effective chiral Lagrangians for nucleon-pion interactions and nuclear forces, *Nucl. Phys.* **B363**, 3 (1991).
- [37] V. Bernard, N. Kaiser, and U.-G. Meissner, Chiral dynamics in nucleons and nuclei, *Int. J. Mod. Phys. E* **04**, 193 (1995).
- [38] E. Epelbaum, H.-W. Hammer, and U.-G. Meissner, Modern theory of nuclear forces, *Rev. Mod. Phys.* **81**, 1773 (2009).
- [39] R. Machleidt and D. R. Entem, Chiral effective field theory and nuclear forces, *Phys. Rep.* **503**, 1 (2011).
- [40] J. Gasser, M. E. Sainio, and A. Svarc, Nucleons with chiral loops, *Nucl. Phys.* **B307**, 779 (1988).
- [41] M. B. Wise, Chiral perturbation theory for hadrons containing a heavy quark, *Phys. Rev. D* **45**, R2188 (1992).
- [42] L. Meng, B. Wang, G.-J. Wang, and S.-L. Zhu, Chiral perturbation theory for heavy hadrons and chiral effective field theory for heavy hadronic molecules, *Phys. Rep.* **1019**, 1 (2023).
- [43] V. Baru, A. A. Filin, C. Hanhart, Y. S. Kalashnikova, A. E. Kudryavtsev, and A. V. Nefediev, Three-body $D\bar{D}\pi$ dynamics for the X(3872), *Phys. Rev. D* **84**, 074029 (2011).
- [44] M. Schmidt, M. Jansen, and H. W. Hammer, Threshold effects and the line shape of the X(3872) in effective field theory, *Phys. Rev. D* **98**, 014032 (2018).
- [45] M.-L. Du, V. Baru, X.-K. Dong, A. Filin, F.-K. Guo, C. Hanhart, A. Nefediev, J. Nieves, and Q. Wang, Coupled-channel approach to T_{cc}^+ including three-body effects, *Phys. Rev. D* **105**, 014024 (2022).
- [46] J. Aguilar and J. M. Combes, A class of analytic perturbations for one-body Schroedinger Hamiltonians, *Commun. Math. Phys.* **22**, 269 (1971).
- [47] E. Balslev and J. M. Combes, Spectral properties of many-body Schroedinger operators with dilatation-analytic interactions, *Commun. Math. Phys.* **22**, 280 (1971).
- [48] T. Myo, Y. Kikuchi, H. Masui, and K. Katō, Recent development of complex scaling method for many-body resonances and continua in light nuclei, *Prog. Part. Nucl. Phys.* **79**, 1 (2014).
- [49] C. E. Thomas and F. E. Close, Is X(3872) a molecule?, *Phys. Rev. D* **78**, 034007 (2008).
- [50] N. Li and S.-L. Zhu, Isospin breaking, Coupled-channel effects and Diagnosis of X(3872), *Phys. Rev. D* **86**, 074022 (2012).
- [51] M. Suzuki, The X(3872) boson: Molecule or charmonium, *Phys. Rev. D* **72**, 114013 (2005).
- [52] Y.-R. Liu, X. Liu, W.-Z. Deng, and S.-L. Zhu, Is X(3872) really a molecular state?, *Eur. Phys. J. C* **56**, 63 (2008).
- [53] A. M. Badalian, L. P. Kok, M. I. Polikarpov, and Y. A. Simonov, Resonances in coupled channels in nuclear and particle physics, *Phys. Rep.* **82**, 31 (1982).
- [54] M. Mai, B. Hu, M. Doring, A. Pilloni, and A. Szczepaniak, Three-body unitarity with isobars revisited, *Eur. Phys. J. A* **53**, 177 (2017).

- [55] H. Xu, B. Wang, Z.-W. Liu, and X. Liu, DD^* potentials in chiral perturbation theory and possible molecular states, *Phys. Rev. D* **99**, 014027 (2019).
- [56] E. Epelbaum, U. G. Meißner, W. Gloeckle, and C. Elster, Resonance saturation for four nucleon operators, *Phys. Rev. C* **65**, 044001 (2002).
- [57] B. Wang, L. Meng, and S.-L. Zhu, $D^{(*)}N$ interaction and the structure of $\Sigma_c(2800)$ and $\Lambda_c(2940)$ in chiral effective field theory, *Phys. Rev. D* **101**, 094035 (2020).
- [58] R. M. More and E. Gerjuoy, Properties of resonance wave functions, *Phys. Rev. A* **7**, 1288 (1973).
- [59] T. Sekihara, Two-body wave functions and compositeness from scattering amplitudes. I. General properties with schematic models, *Phys. Rev. C* **95**, 025206 (2017).
- [60] X.-W. Kang, J. Haidenbauer, and U.-G. Meißner, Antinucleon-nucleon interaction in chiral effective field theory, *J. High Energy Phys.* **02** (2014) 113.
- [61] C. Hanhart, Y. S. Kalashnikova, P. Matuschek, R. V. Mizuk, A. V. Nefediev, and Q. Wang, Practical parametrization for line shapes of near-threshold states, *Phys. Rev. Lett.* **115**, 202001 (2015).
- [62] B. Wang, Z.-W. Liu, and X. Liu, $\bar{B}^{(*)}\bar{B}^{(*)}$ interactions in chiral effective field theory, *Phys. Rev. D* **99**, 036007 (2019).
- [63] N. Li, Z.-F. Sun, X. Liu, and S.-L. Zhu, Coupled-channel analysis of the possible $D^{(*)}D^{(*)}$, $\bar{B}^{(*)}\bar{B}^{(*)}$ and $D^{(*)}\bar{B}^{(*)}$ molecular states, *Phys. Rev. D* **88**, 114008 (2013).
- [64] X. Liu, Y.-R. Liu, W.-Z. Deng, and S.-L. Zhu, $Z^+(4430)$ as a $D_1'D^*(D_1D^*)$ molecular state, *Phys. Rev. D* **77**, 094015 (2008).
- [65] B. Wang, L. Meng, and S.-L. Zhu, Hidden-charm and hidden-bottom molecular pentaquarks in chiral effective field theory, *J. High Energy Phys.* **11** (2019) 108.